Check for updates

Green synthesis of carbon quantum dots from nutshells for enhanced performance in dye-sensitized solar cells

Yang Yu, [ID] [a] Yuxia Ouyang,[a] Fei Xu,[a] Tiefeng Wang,[a] Xiaoyan Wei,[a] Tongtong Wang [ID] *[a] and Yi Yao*[b]

This study presents a sustainable approach to large scale synthesis of carbon quantum dots (CQDs) from nutshells, a widely available waste from biomass, using hydrogen peroxide (H_2O) as the oxidizing agent in a hydrothermal process. The conditions of synthesis, including concentration of H_2O_2, reaction temperature and time, have been systematically optimized. The results show that optimal conditions include a concentration of 2.5% H_2O_2, a reaction temperature of 180 °C and a reaction time of 12 hours. The obtained CQDs have an average size of 3 nm and excellent fluorescence. The 2 L Parr reactor has been used to increase the production process and make it more viable for industrial applications. By-products of the reaction, including gas, liquid and solid residues, have been analyzed to understand the distribution of carbon. In addition, CQDs have been incorporated in dye-sensitive solar cells (DSSCs) where they have significantly improved the photovoltaic performance, with increased current density and overall efficiency. This work highlights the potential of biomass-based CQDs for the sustainable production of nanomaterials and for energy conversion applications, and offers a scalable and environmentally friendly alternative to synthesis of CQDs.

Introduction

The growing demand for sustainable and environmentally friendly materials has stimulated a strong interest in developing renewable sources for the synthesis of nanomaterials, in particular carbon quantum dots (CQDs).[1,2] These materials are gaining attention due to their exceptional optical properties, including strong photoluminescence, excellent biocompatibility, and ease of functionalization.[3–5] As a result, CQDs are considered as ideal candidates for a variety of applications, including energy-recovery devices, bioimaging and sensors.[6,7] Despite these promising characteristics, challenges such as low yield, high cost, and environmental impact of conventional synthesis methods hinder their large-scale use.

Traditional CQD synthesis methods can be classified as top-down or bottom-up approaches.[8,9] Top-down techniques, such as laser ablation,[10] chemical oxidation,[11] electrochemical oxidation,[12] and ultrasonic-assisted synthesis,[13] involve breaking down bulk carbon materials to form CQDs. Although these methods provide accurate control of the size and surface properties of CQDs, they often require high energy inputs, toxic substances, and specialized equipment, which limits their

scalability and environmental sustainability. For example, chemical oxidation of graphite using strong oxidizing agents like nitric acid (HNO_3) or sulfuric acid (H_2SO_4) may produce high-quality CQDs, but also generate large amounts of hazardous waste.[14] Bottom-up methods, such as hydrothermal synthesis,[15] thermal decomposition,[16] and microwave-assisted synthesis[17] offer more eco-friendly and versatile options for CQD production but are often limited by low yields and difficulties in scaling up to industrial scale. In particular, hydrothermal synthesis has been extensively investigated because of its simplicity and the ability to produce CQDs with tunable sizes and properties. However, many of these methods rely on high purity carbon sources and are often hampered by low yields and difficulties in scaling up to the level of industrial production.[18] Although microwave assisted synthesis has shown promising results in improving energy efficiency, scalability and costs remain major concerns.[19]

Researchers have recently looked to biomass waste as a potential substitute carbon source for the synthesis of CQDs. The use of materials like fruit peels, nutshells, and other agricultural residues not only solves important waste disposal issues but is also economical and renewable.[20,21] In particular, nutshells are a great option because of their high carbon content, affordability, and accessibility as agricultural by-products.[22] Research has demonstrated that CQDs made from biomass, particularly when produced hydrothermally, have exceptional photoluminescent qualities, which increases their

[a]*College of Advanced Materials Engineering, Jiaxing Nanhu University, Jiaxing, Zhejiang 314001, China. E-mail: wtt@jxnhu.edu.cn*

[b]*School of Energy Resources, University of Wyoming, Laramie, WY 82071, USA. E-mail: yyao1@uwyo.edu*

potential for application in energy devices.[23,24] However, small-scale laboratory reactions are frequently used in current research on biomass-derived CQDs, which is insufficient to address the issues of scalability, efficiency, and cost-effectiveness. Furthermore, the carbon balance during the synthesis process has received less attention than the optical and electronic characteristics of CQDs, which have been the subject of much research. Optimizing the yield and quality of the CQDs and facilitating large-scale production depend on an understanding of how carbon is distributed across the gas, liquid, and solid phases.

This study aims to bridge this gap by presenting a detailed investigation of the synthesis process of CQDs from nutshells using a hydrothermal method, focusing on the optimization of the conditions for synthesis such as reaction time, temperature and the concentration of hydrogen peroxide. Notably, the study uses the 2 L Parr reactor to increase the efficiency of the process and make it more viable for industrial applications. In addition, we have incorporated synthesized CQDs into dye-sensitive solar cells (DSSCs) and have seen significant improvements in photovoltaic performance. These findings highlight the potential of biomass-based CQDs for the production of large-scale, sustainable nanomaterials, providing an environmentally friendly alternative to traditional synthesis methods and opening the door to wider industrial applications.

Experimental section

Materials

Pecan nutshells were purchased from Millican Pecan Company and used as raw materials and carbon sources. The ultimate analysis was performed using ASTM D4239-18e1, and D5373-21 methods. The proximate analysis was carried out according to ASTM D5016-16 and D5142-90(1998) methods. The obtained pecan nutshells were ground and sieved to 200 mesh (74 μm) and dehydrated at 80 °C for 12 h before being used for the experiment. 30 wt% hydrogen peroxide (H_2O_2, ACS grade) was purchased from Fisher Scientific. TiO_2 paste was purchased from Solaronix (part number 14411). High purity nitrogen gas (N_2, UHP, 99.999%) was provided by US Welding. All materials were used without further purification.

CQDs synthesis method

A 4848 controller was used to load 10 g of nutshell (m_0) into the 2 L high-pressure stainless-steel reactor. For every batch, the reactant consisted of roughly 1.5 L of a particular concentration of H_2O_2 water solution. Before beginning the reaction, 1 L min^{-1} N_2 was purged into reactor for 30 minutes to get rid of any leftover air. To calculate and quantify the gaseous products, the residual N_2 was also utilized as an internal standard. Afterwards, the reactor was heated to a range of temperatures between 90 and 210 °C while being subjected to various reaction conditions. The reaction time was set at two to twelve hours. Using gas chromatography, the gaseous products were examined. A 47 mm glass vacuum filtration apparatus with 0.45 μm Teflon filter paper was used to separate the mixture that was left

in the reactor. After the separated solid residue was dried for 24 hours at 90 °C in an oven, it was weighed and designated as m_1. TGA was used to determine the nutshell's ash content. Consequently, weight loss was used to calculate the nutshell conversion by

$$x\ (\%) = \frac{(w_0 - d)(w_1 - d)}{(w_0 - d)} \times 100\% \qquad (1)$$

where x (%) is the nutshells conversion, w_0 is nutshells' initial weight without moisture, w_1 is collected unreacted nutshells without moisture, and d is nutshells' ash content.

Gas products were collected and quantitatively analyzed by online gas chromatography (Agilent 8890 GC System). Thus, the total carbon in gas products can be calculated. The total carbon in the liquid solution was measured by the TOC instrument (Shimadzu – Total Organic Analyzer Model: TOC-V csh/csn), and the residue carbon was tested by the elemental analyzer (Elementar Analysensysteme GmbH-Vario MACRO Cube Elemental Analyzer).

Characterizations

The ultimate analysis of the nutshells was conducted in accordance with ASTM D5373-21 using a Vario MACRO Cube Elemental Analyzer. The oxygen content was determined by the difference method. Thermogravimetric analysis (TGA) was performed using a TA SDT-Q600 to assist in determining the ultimate analysis of the nutshells. High-resolution transmission electron microscopy (HR-TEM, JEOL JEM-2100) was employed to characterize the morphology and size distribution of the obtained CQDs. To investigate the photophysical properties, 3D fluorescence spectroscopy was carried out using a Horiba Fluorolog-3 spectrofluorometer at 25 °C. The excitation wavelength range was set from 200 to 600 nm with 4 nm intervals, and the emission wavelength range was adjusted from 296 to 700 nm with 2 nm intervals for steady-state fluorescence excitation and emission measurements. Data collection and analysis were performed using OriginLab 8.0 software. The functional groups of the synthesized CQDs were analyzed using Nicolet iS50 Fourier transform infrared (FT-IR) spectroscopy with a nondestructive attenuated total reflectance (ATR) technique. The samples were scanned 64 times with a resolution of 16 cm^{-1}, within a wavenumber range of 4000 to 400 cm^{-1}. The phase composition and presence of graphitic carbon were confirmed using Rigaku X-ray diffraction (XRD) in the 2θ range from 5° to 45°, employing Cu-Kα radiation at 40 kV and 40 mA.

Fabrication of semiconductor photoanodes and DSSCs assembly

The CQD solution was diluted 50-fold, and the doctor's blade technique was employed to apply the paste onto 1.5 cm × 2.0 cm conductive FTO glass substrates (Sigma-Aldrich). The coated glasses were then heat-treated at 500 °C for 1 hour, followed by cooling to room temperature. The coating procedure was repeated, and the samples were calcined again. Three drops of the CQD solution were added to the paste, and the films were dried at 90 °C. Afterward, the glasses were immersed in a 1 mM

N3 dye solution (Sigma-Aldrich) for 24 hours to create the photoanodes. For DSSC assembly, the photoanode and a Pt-coated FTO glass cathode (1.5 cm × 2.0 cm) were aligned and separated by a 3.5-mil spacer (1 cm × 1 cm Kapton polyimide film), which had a hole for the iodolyte Z-50 electrolyte (Solaronix). The electrodes were fastened with binder clips.

The electrochemical performance of the DSSCs was assessed under 1.5 AM solar irradiation (DAIEL LSH-7520, 100 mW cm^{-2}). Linear sweep voltammetry (LSV) measurements were conducted using a CHI6203D electrochemical analyzer, scanning from −1 to 1 V at 0.02 V s^{-1}. The photo-conversion efficiency (η) was calculated using eqn (2)–(4).

$$P = V \times j = V \times I/A; \quad (2)$$

$$FF = \frac{P_{max}}{V_{oc} \times J_{sc}}; \quad (3)$$

$$\eta \ (\%) = \frac{P_{max}}{P_{in}} \times 100\%. \quad (4)$$

Here, P is the power intensity of the DSSC (mW cm^{-2}), V is the voltage between the working and reference electrodes (V), j denotes the current density (mA cm^{-2}), I is the measured current at V (mA), A is the area of the active area (cm^2), FF is the fill factor; P_{max} is the maximum power intensity (mW cm^{-2}), J_{sc} is the short-circuit current density (mA cm^{-2}), V_{oc} is the open-circuit voltage (V), and P_{in} is the incident light power intensity (mW cm^{-2}). Finally, η represents the photo-conversion efficiency.

Result and discussion

Nutshell analysis

The proximate and ultimate analyses of pecan nutshells were conducted to understand their chemical composition and energy content, and the results are presented in Table 1. The moisture, volatile matter, and ash contents of the nutshells were determined to be 5.03%, 60.49%, and 2.1%, respectively. The fixed carbon content, measured by thermogravimetric analysis (TGA), was 32.38%, indicating that the nutshells have a significantly higher volatile content and a lower fixed carbon fraction. An elemental analysis, based on organic matter, revealed the following composition: 53.67% carbon, 5.64% hydrogen, 0.8% nitrogen, 0.57% sulfur, and 39.32% oxygen. The presence of inorganic compounds in the nutshells may also be important for CQD synthesis, as certain metals could participate in reactions with hydrogen peroxide (H_2O_2) as catalysts.[25]

Table 2 Major elements in nutshell ash

Element	(wt%)	Oxide	(wt%)
Si	11.8	SiO_2	17.65
Al	1.45	Al_2O_3	3.81
Fe	2.09	Fe_2O_3	4.18
Mg	4.43	MgO	5.24
Ca	15.83	CaO	15.48
Ti	0.43	TiO_2	0.51
K	30.29	K_2O	50.96
Na	0.69	Na_2O	1.30
Mn	0.73	MnO_2	0.81
Ba	0.07	BaO	0.05

The composition of the ash was determined by inductively coupled plasma mass spectrometry (ICP-MS), and main components of the ash are shown in Table 2. The weight percentages of the elements are as follows: Si = 11.8%, Al = 1.45%, Fe = 2.09%, Mg = 4.43%, Ca = 15.83%, Ti = 0.43%, K = 30.29%, Na = 0.69%, Mn = 0.73%, and Ba = 0.07%.

Fig. 1a shows the profile of the thermogravimetric analysis (TGA) of the sample of the nucleus recorded from ambient temperature to 1000 °C under a nitrogen flow of 100 mL min^{-1} at a heating rate of 10 °C min^{-1}. This analysis provides insight into the thermal decomposition behavior of the nutshells, which is necessary to assess their potential as carbon precursors for the synthesis CQDs. Three main stages of weight loss were observed: (1) a primary weight loss from 25 to 200 °C with a 6.69% weight loss, attributed to moisture removal;[26] (2) the primary weight loss, occurring between 200 and 400 °C, resulting in a 40.51% weight loss due to the thermal degradation of the main organic components in the pulp, such as cellulose, hemicellulose and lignin;[27,28] and (3) a gradual weight loss above 400 °C, leading to the formation of a stable solid carbon structure derived from lignin. Although the thermal degradation pattern of the nutshells does not directly relate to the temperature conditions used for the synthesis of CQDs, the TGA profile provides valuable information on the organic composition and structural stability of precursors.

Fourier transform infrared spectroscopy (FTIR) has been used to further understand functional groups and chemical bonds present in nutshells. Fig. 1b shows the FTIR results of the raw nutshell sample. The broad peak at approximately ~3400 cm^{-1} corresponds to the –OH bond, which is typically associated with moisture in the sample. The peak at ~2932 cm^{-1} is attributed to hydrogen in substituted aromatic

Table 1 Proximate and ultimate analyses of nutshells

Proximate analysis (wt%)			Ultimate analysis (wt%, daf)				
M_{ad}	A_d	V_{daf}	C	H	N	S	O^a
5.03	2.1	60.49	53.67	5.64	0.8	0.57	39.32

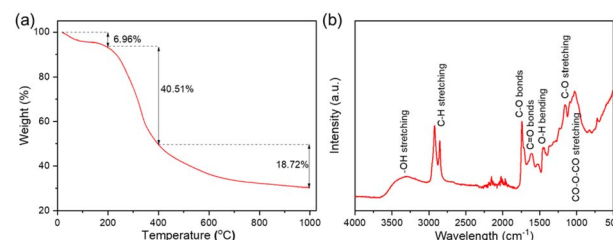^{a} Calculated by difference.

Fig. 1 (a) TGA and (b) FTIR analysis of nutshell.

rings, and the more intense aromatic C–H peak further indicates the aromatic nature of the nutshells. Two prominent peaks at 1736 cm^{-1} and 1610 cm^{-1} are attributed to the C=O bonds in carbonyl and carboxyl groups,[29,30] with the intensity of these peaks reflecting the high oxygen content in the nutshells. This is further supported by another peak around ~1040 cm^{-1}, which is attributed to CO–O–CO structural bending.[31] The FTIR analysis is crucial for identifying functional groups in the nutshells, which may play a role in the subsequent synthesis of CQDs, particularly in terms of interactions with the oxidizing agent, H_2O_2, and the formation of specific carbon-based structures.

CQDs synthesis condition

Nutshell-derived CQDs have been extensively studied, with a focus on various nutshell sources, synthesis methods, separation techniques, and product tuning (such as size, structure, and surface functional groups). These CQDs have found applications in a wide range of fields.[2] However, most of the existing studies primarily concentrate on the characterization and applications of the CQDs, while little attention has been given to investigating the underlying reaction process, such as the carbon balance and by-products. These factors are crucial for the industrial-scale production of CQDs. In this study, we utilize nutshells as a carbon source and replace traditional acidic reactants with hydrogen peroxide (H_2O_2) in a sealed hydrothermal reactor to produce CQDs. The optimized synthesis conditions, including reaction time, temperature, and H_2O_2 concentration, are systematically explored. In addition, the reaction by-products—comprising gases, liquids, and solid residues—are collected and analyzed to better understand the reaction process. The photophysical properties of the synthesized CQDs were investigated using UV-Vis and fluorescence spectroscopy to understand their optical characteristics and evaluate their potential for applications in energy conversion devices like DSSCs.

Effect of the H_2O_2 concentration

H_2O_2 plays a crucial role as an oxidizing agent in this reaction, effectively breaking down the organic matter in biomass. Compared to commonly used acids, H_2O_2 offers the advantage of a lower environmental impact and higher reaction activity. To determine the optimal concentration of H_2O_2 for this process, 10 g of pretreated nutshell samples were reacted with 1.5 L of H_2O_2 solution in a 2 L reactor. Five distinct H_2O_2 concentrations ranging from 1.5% to 3.5% were tested, at a reaction temperature of 180 °C for 12 hours. The results, shown in Fig. 2, provide insights into the carbon distribution across the gas, solution, and residue phases.

As the concentration of H_2O_2 increased from 1.5% to 2.5%, the carbon content in the residue decreased significantly from 39.25% to 21.79%. However, with further increases in H_2O_2 concentration, the residue carbon content remained relatively stable at 19.7% when the concentration reached 3.5%. The carbon content in the solution increased from 31.62% to 34.77% as the H_2O_2 concentration was increased from 1.5% to
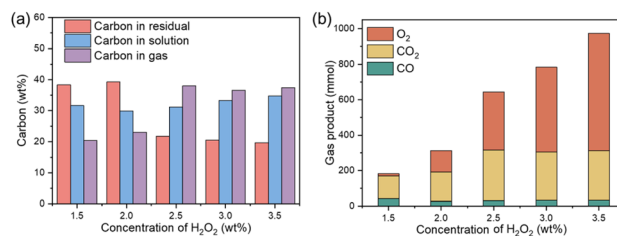

Fig. 2 (a) Distribution of carbon across the gas, residual, and solution phases in the final products. (b) Distribution and composition of the gas products. The reactions were conducted for 12 hours at 180 °C with H_2O_2 concentrations ranging from 1.5% to 3.5%.

3.5%. A notable rise in the total carbon content in the gaseous products was observed, from 20.42% at 1.5% to 38.05% at 2.5%, before slightly decreasing to 34.77% at 3.5% H_2O_2. These results suggest that a 2.5% H_2O_2 solution concentration is optimal for CQD production using nutshells as the carbon source. Beyond this concentration, further increases in H_2O_2 lead to a shift in the composition of the gaseous products, where O_2 becomes the dominant component. The increase in O_2 content, from 11.68 mmol to 661.07 mmol, indicates that the oxidation process between the nutshells and H_2O_2 is intensified with higher concentrations of H_2O_2. This change is likely due to the self-decomposition of H_2O_2. In conclusion, when the H_2O_2 concentration exceeds 2.5%, the decomposition of H_2O_2 becomes the dominant reaction, contributing to chemical waste in the form of excess oxygen. Moreover, the use of higher H_2O_2 concentrations, while potentially enhancing oxidation, increases the cost of the process, as H_2O_2 is significantly more expensive than the raw nutshell material. Additionally, the consumption of H_2O_2 limits its availability for the desired reactions, reducing process efficiency. Therefore, a concentration of 2.5% H_2O_2 strikes a balance between efficient CQD synthesis and cost-effectiveness.

CQDs synthesized under different H_2O_2 concentrations (1.5% to 3.5%) exhibit different optical properties as demonstrated by the UV-Vis and the photoluminescence (PL) characterization as shown in Fig. 3. UV-Vis spectroscopy provides insight into the electronic structure and absorption properties, while PL spectroscopy provides information on the emission behavior dependent on excitation, both of which are important for understanding the photophysical properties of CCDs.[32] As the H_2O_2 concentration increases, the color of the CQDs transitions from light yellow for the 1.5% sample to deep yellow for the 2.5% sample, and then back to light yellow with further increasing concentration. Under 365 nm UV light irradiation, all samples show blue fluorescence, the intensity of the fluorescence gradually increasing and decreasing, with the strongest blue emission occurring in the 2.5% sample. UV-Vis spectroscopy reveals similar absorption characteristics for all CQD samples in the 200–300 nm range with two major absorption peaks, one at 230 nm and another at 280 nm, indicating the presence of the $\pi \rightarrow \pi$ transitions* in the carbon core and n $\rightarrow \pi$ transitions* related to the surface groups, respectively.[33] As H_2O_2 concentrations increased, significant changes in absorption spectra were observed. In particular, the
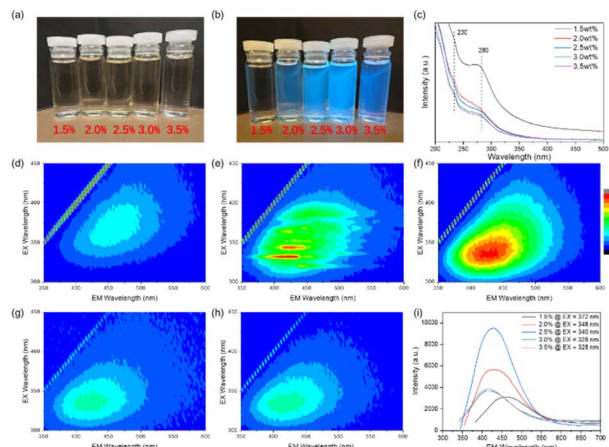
Fig. 3 (a) Images of the samples in daylight and (b) under 365 nm UV light exposure. (c) UV-Vis absorption spectra of the obtained samples. (d–h) 3D fluorescence spectra of CQD-containing solutions and reaction products at varying H_2O_2 concentrations (1.5–3.5%) after 12 hours at 180 °C: (d) 1.5%, (e) 2.0%, (f) 2.5%, (g) 3.0%, (h) 3.5%, and (i) emission spectra of each system at their respective excitation maxima.

absorption band of the $\pi \rightarrow \pi$ absorption band* at 230 nm became weaker, while the $n \rightarrow \pi$ transition* at 280 nm became more intense. This behavior may be attributed to the increased structural order of CQDs with higher H_2O_2 concentrations, which may decrease the number of functional surface groups and result in a higher number of conjugated structures in CQDs.

The 3D PL spectra exhibit typical excitation-dependent photoluminescence behavior, with the emission intensity increasing as the excitation wavelength ranges from 300 nm to 450 nm shown in Fig. 3d–i. The trend of the maximum emission peaks is consistent with fluorescence intensity, and the CQDs synthesized with 2.5% H_2O_2 at 180 °C exhibited the most blue fluorescence. At excitation wavelengths of 375 nm, 348 nm, 340 nm, 328 nm, and 328 nm, the optimal PL emission peaks for 1.5%, 2.0%, 2.5%, 3.0%, and 3.5% H_2O_2 are found at 464 nm, 438 nm, 428 nm, 418 nm, and 418 nm, respectively. With increasing H_2O_2 concentration, both the excitation and emission peaks shift to shorter wavelengths. Thus, the 2.5% H_2O_2 concentration is the optimal condition for synthesizing CQDs, offering the strongest fluorescence and ideal absorption properties.

Effect of the reaction temperature

The reaction temperature plays a critical role in the synthesis of CQDs. 10 g of nutshells were added to a reactor with 1.5 L of a 2.5% H_2O_2 solution, and the reaction was conducted for 12 hours at temperatures of 90 °C, 120 °C, 150 °C, 180 °C, and 210 °C, separately. The findings, which are displayed in Fig. 4, show that the residual carbon content significantly decreases as the temperature rises, going from 60.32% at 90 °C to 14.54% at 210 °C. According to the Arrhenius equation, the nutshell conversion rate was highest at 210 °C. The nutshells converted more quickly as a result of the reaction rate staying constant as
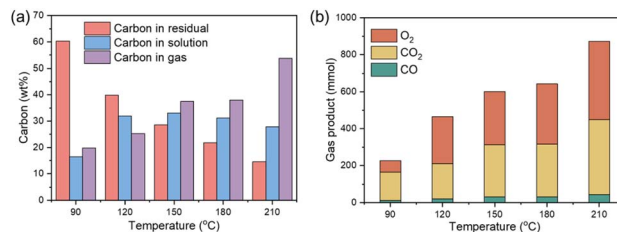

Fig. 4 (a) Distribution of carbon in the gas, residual, and solution phases of the final products; (b) distribution and composition of the gas products. The reactions were conducted for 12 hours with 2.5% H_2O_2 at varying temperatures (90–210 °C).

the temperature rose. At 180 °C, the carbon content of the solution rose from 16.46% to 33.06%, and then at 210 °C, it decreased to 27.86%. According to this pattern, organic carbon continuously reacts with H_2O_2 at higher temperatures, eventually turning into gas. The gaseous products, including O_2, CO_2, and CO, showed a positive correlation with temperature. Higher temperatures accelerated the breakdown of chemical bonds in the organic components of the nutshells, as well as the self-decomposition of H_2O_2. The production of a considerable amount of O_2 and CO_2 at 210 °C suggested that the reaction was dominated by the breakdown of H_2O_2. Elevated temperatures therefore encourage the breakdown of the nutshells and H_2O_2, resulting in a larger gas release. Higher temperatures cause carbon to be lost as gaseous byproducts, even though they also increase conversion efficiency. This emphasizes the necessity of reaction temperature optimization to minimize carbon loss to gas and balance CQD yield.

The CQDs synthesized at various temperatures (90 °C to 210 °C) exhibit significant changes in optical properties shown in Fig. 5. As the reaction temperature increases, the color of the CQDs changes from light yellow at 90 °C to deep yellow at 180 °
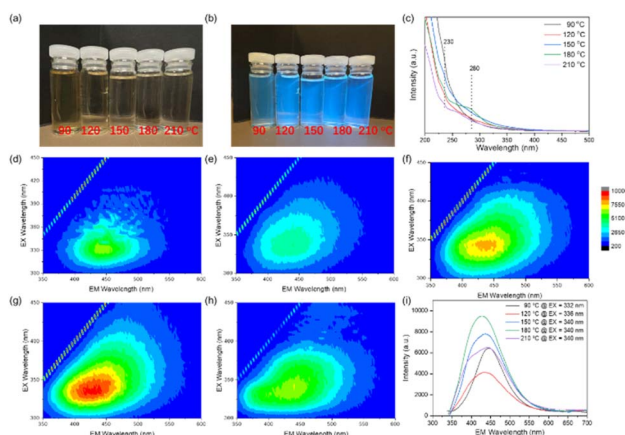

Fig. 5 (a) Images of the samples in daylight and (b) under 365 nm UV light exposure. (c) UV-Vis absorption spectra of the obtained samples. (d–h) 3D fluorescence spectra of CQD-containing solutions and reaction products at different temperatures (90–210 °C) after 12 hours with 2.5% H_2O_2: (d) 90 °C, (e) 120 °C, (f) 150 °C, (g) 180 °C, (h) 210 °C, and (i) emission spectra of each system at their respective excitation maximum.

C, and then back to light yellow as the temperature rises further. Under 365 nm UV light irradiation all samples show blue fluorescence, with increasing fluorescence intensity first and decreasing intensity thereafter. The sample synthesized at 180 °C exhibits the strongest blue fluorescence. When the temperature increased from 90 °C to 210 °C, the UV-Vis absorption spectra showed a decrease in the intensity of the absorption peaks at 230 nm and 280 nm, with the peaks becoming less pronounced. At lower temperatures (e.g., 120 °C), the $\pi \rightarrow \pi$ transition* at 230 nm dominated, reflecting less structural order in the CQDs, which is typical for CQDs with more surface defects. As the temperature increased, the absorption peak at 230 nm became less pronounced, and the $\pi \rightarrow \pi$ absorption band* shifted towards higher energy, becoming less prominent. This suggests that the CQDs formed at higher temperatures (e.g., 180 °C to 210 °C) exhibited more conjugated structures with fewer defects, contributing to a stronger n → π transition* at 280 nm, indicative of a more ordered and graphitic core structure. When the temperature was increased from 90 °C to 210 °C, the UV-Vis absorption spectra showed a shift in the intensity of the absorption peaks at 230 nm and 280 nm.

The 3D PL spectra showed a similar trend shown in Fig. 5d–i. At lower temperatures, the fluorescence intensity was relatively weak, with a larger emission peak at longer wavelengths. As the temperature increased, the fluorescence intensity enhanced, and the emission shifted to shorter wavelengths. The CQDs synthesized at 180 °C exhibited the highest fluorescence intensity. At excitation wavelengths of 332 nm, 336 nm, 340 nm, 340 nm, and 340 nm, the optimal PL emission peaks for the 90 °C, 120 °C, 150 °C, 180 °C, and 210 °C samples are located at 484 nm, 436 nm, 436 nm, 428 nm, and 440 nm, respectively. As the reaction temperature increases, the excitation wavelength increases, while the optimal emission wavelength shifts to shorter wavelengths, likely due to the increase in CQD particle size and the formation of surface C=O functional groups, which is consistent with the UV-Vis results. In conclusion, reaction temperature plays a pivotal role in tuning the photophysical properties of CQDs. The optimal synthesis temperature appears to be around 180 °C, where the CQDs exhibit the strongest fluorescence and a more stable, controllable structure.

Effect of reaction time

The effect of the reaction time on the formation of CQD was investigated in the range of 2 to 12 hours. In this experiment, 10 g of the sample of nutshells were mixed with 1.5 L of the solution of 2.5% H_2O_2 solution and reacted at 180 °C for varying durations. The distribution of carbon in the gas, liquid, and residue phases is shown in Fig. 6a. The carbon content in the residue decreased from 26.38% after 2 hours to 22.34% after 6 hours, and then slightly reduced further to 21.79% after 12 hours. This trend suggests that the decomposition of organic matter predominantly occurs during the first 6 hours of the reaction. The carbon content in the solution initially increased from 41.57% to 42.38% between 2 and 4 hours, but subsequently decreased as the reaction time continued, reaching
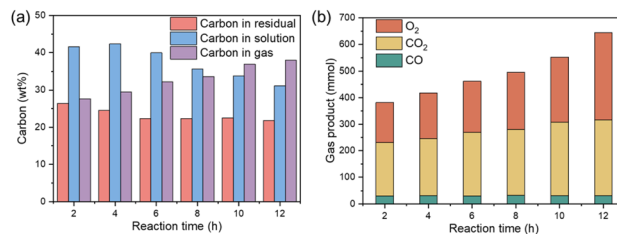

Fig. 6 (a) Distribution of carbon in the gas, residual, and solution phases of the final products; (b) distribution and composition of the gas products. The reaction was conducted with 2.5% H_2O_2 at 180 °C for varying reaction times (2–12 hours).

31.15% at 12 hours. This suggests that after an initial increase in the dissolved carbon, the process stabilizes, and carbon compounds are increasingly converted into gaseous products. The carbon content in the gas phase continued to rise with reaction time, with both CO_2 and O_2 levels showing significant changes, as depicted in Fig. 6b. This observation indicates that extended reaction times lead to a greater amount of carbon being converted to the gas phase. Additionally, prolonged reaction times promote the self-decomposition of H_2O_2, resulting in increased energy consumption. Despite these changes, an optimal reaction time is essential for maximizing CQD yield and quality. Small carbon molecules require sufficient time to aggregate and form CQDs under hydrothermal conditions. Furthermore, the removal of small dissolved carbon molecules, such as formic acid and acetic acid, occurs over time, further improving the quality of the synthesized CQDs. Therefore, while longer reaction times enhance the conversion to gaseous products, they also allow for better formation and purification of the CQDs.

As shown in Fig. 7, the reaction time plays a crucial role in determining the photophysical properties of CQDs synthesized from nutshells. The six CQDs samples synthesized under
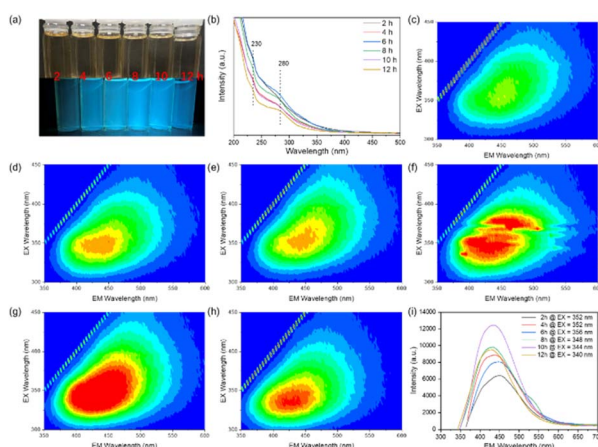

Fig. 7 (a) Images of the samples in daylight and under 365 nm UV light exposure. (b) UV-Vis absorption spectra of the obtained samples. (c–h) 3D fluorescence spectra of CQD-containing solutions and reaction products at varying times (2–12 hours) with 2.5% H_2O_2 at 180 °C: (c) 2 hours, (d) 4 hours, (e) 6 hours, (f) 8 hours, (g) 10 hours, and (h) 12 hours, and (i) emission spectra of each system at their respective excitation maxima.

different reaction times (2–12 hours) all appear yellow. Under 365 nm UV light irradiation, all samples exhibit blue fluorescence, with the fluorescence intensity initially increasing and then decreasing. The sample synthesized for 10 hours shows the strongest blue fluorescence. The UV-Vis absorption spectra in Fig. 7b reveals that at shorter reaction times (*e.g.*, 2 hours), the CQDs exhibited weak fluorescence with a broad emission peak and a dominant 230 nm absorption, indicating smaller or disordered CQDs. As the reaction time increased to 6 hours, the absorption at 280 nm became more pronounced, suggesting the formation of conjugated structures and fewer surface defects. After 12 hours, the spectra showed a strong 280 nm peak and a weaker 230 nm peak, indicative of a more ordered, graphitic core structure. Beyond 12 hours, the peaks broadened, signaling aggregation and increased heterogeneity in CQD size.

In parallel, the 3D PL spectra revealed significant evolution in fluorescence properties with reaction time shown in Fig. 7c–f. At 2 hours, the CQDs exhibited weak fluorescence with a broad emission peak at 450 nm, characteristic of smaller, less ordered structures. As the reaction progressed to 6 hours, fluorescence intensity increased, and the emission peak shifted to 438 nm. At 10 hours, the CQDs displayed the highest fluorescence intensity with an emission peak at 434 nm, suggesting optimal formation of emissive states. However, at 12 hours, fluorescence intensity began to decline, accompanied by a slight blue shift to 440 nm, likely due to CQD aggregation and oxidation, leading to self-quenching and reduced photoluminescence efficiency. Additionally, the increase in PL intensity over time may be partially attributed to higher CQD concentrations in solutions. Considering the pronounced absorption peak at 280 nm and the balance between fluorescence efficiency and concentration effects, 12 hours appears to be the optimal reaction time for CQD synthesis.

Characteristics of CQDs sample

Fig. 8 displays the TEM images of carbon quantum dots (CQDs) synthesized under optimized conditions using 10 g of nutshells and 1.5 L of a 2.5% hyd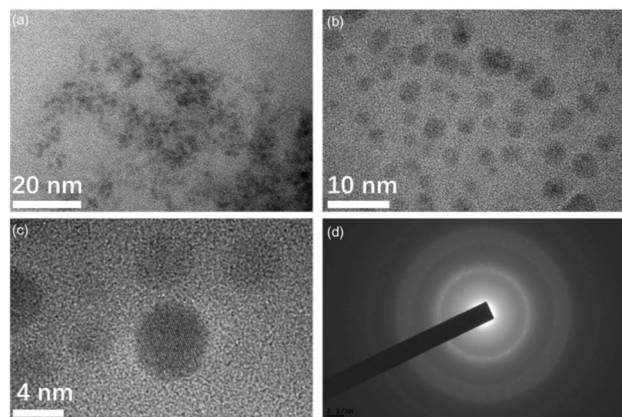rogen peroxide (H_2O_2) solution, reacting for 12 hours at 180 °C. The resulting CQDs are spherical in shape and exhibit excellent dispersion in water, with particle sizes ranging from 2 to 6 nm, and an average diameter of approximately 3 nm. The core structure of these CQDs is primarily π-conjugated, with a surface that is amorphous and rich in oxygen-containing functional groups, such as hydroxyl, carboxyl, and epoxide groups, which are essential for improving their solubility and functionality. This is further confirmed by the selected area electron diffraction (SAED) pattern shown in Fig. 8d, which reveals well-defined diffraction rings corresponding to the (100) and (110) planes of graphite, indicating the presence of crystallinity within the carbon core.[34] These rings demonstrate the degree of order in the CQD structure, which is crucial for their optical properties. The CQDs exhibit strong blue fluorescence, which is enhanced by their small particle size and the presence of surface-related electronic transitions.[35] The functionalization of the CQD surface with oxygen-containing groups significantly influences their chemical reactivity, making them ideal for applications in energy conversion devices, bioimaging, and other advanced technologies.[36]

The FTIR spectrum and XRD pattern of the CQD powder, shown in Fig. 9, provide valuable insights into the chemical composition and crystalline of the CQDs. A broad peak in the range of 2600–3000 cm^{-1} corresponds to the O–H stretching vibration, indicating abundant oxygen-containing groups on the surface of the CQDs. The peak at 1624 cm^{-1} suggests conjugated carbon structures (C=C), which are crucial for the CQDs' optical and electronic properties.[37] Peaks between 1300 cm^{-1} and 1000 cm^{-1} are linked to the C–O bond, confirming oxygen functionality on the CQD surface.[38] These findings align with the TEM analysis, where the spherical CQDs exhibit an ordered core structure, largely attributed to the C=C band. The oxygenated groups, such as hydroxyl and carboxyl, introduced during the H_2O_2 oxidation process, are crucial for enhancing the hydrophilicity and dispersibility of the CQDs in aqueous solutions. Additionally, the XRD pattern confirms the crystalline nature of the CQD core, showing diffraction peaks consistent with graphite-like domains. These peaks suggest that the CQDs possess partial crystallinity, contributing to their photoluminescent properties. These characteristics make the CQDs highly suitable for various applications, including energy conversion devices and bioimaging.

The photostability of CQDs is crucial for their applications in bioimaging, sensing, and optoelectronics. In Fig. 10, the
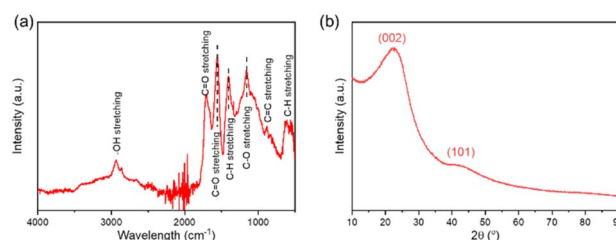

Fig. 8 (a) TEM image of CQDs; (b and c) HRTEM images of CQDs; (d) SAED pattern of CQDs derived from nutshells prepared with 2.5% H_2O_2 at 180 °C for 12 hours.

Fig. 9 (a) FTIR spectrum and (b) XRD pattern of CQDs prepared from nutshells with 2.5% H_2O_2 at 180 °C for 12 hours.

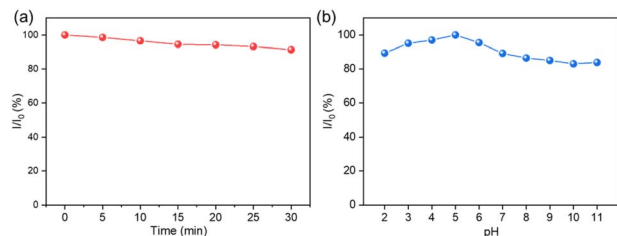**Fig. 10** Photostability test of CQDs under continuous irradiation with 365 nm light (a) and at pH values ranging from 2 to 11 (b).

Table 3 Electrochemical test results of solar cells sensitized by CQD and dyes, and comparative analysis with existing methods

Sample	V_{oc} (V)	J_{sc} (mA cm^{-2})	FF	E_{ta}	Ref.
N3 only	0.63	6.41	0.66	2.66%	This work
N3 and CQDs	0.64	7.05	0.68	3.08%	This work
N-719 only	0.73	13.5	0.74	7.30%	40
N-719 and N-CQDs	0.73	15.0	0.75	8.20%	40
N719 only	0.70	15.77	0.70	7.8%	41
N719 and S-CQD	0.68	17.01	0.70	8.19%	41

photostability of the prepared CQDs was evaluated under continuous 365 nm light irradiation and across a pH range of 2 to 11. The results revealed a gradual decline in fluorescence intensity under prolonged UV exposure, indicating photo-degradation, likely due to photo-oxidation.[39] Furthermore, the CQDs exhibited pH-dependent fluorescence behavior, with reduced fluorescence at extreme acidic (pH 2) and alkaline (pH 11) conditions. This suggests that their optical properties are influenced by changes in surface charge or structure under varying pH levels. These findings are in agreement with previous studies, which demonstrated good stability under UV irradiation, highlighting the potential of CQDs for applications that require stable fluorescence properties under both UV exposure and diverse pH conditions.

CQDs doped TiO$_2$ to DSSCs

Fig. 11 and Table 3 illustrate the performance of carbon quantum dots (CQDs) as a co-sensitizer in photoanodes for dye-sensitized solar cells (DSSCs). The current–voltage (j–V) curves and the performance of solar cells with different photoanodes were compared. When only TiO$_2$ was applied (empty), there was no short-circuit current J_{sc} under both dark and light conditions. However, with N3 dye, the J_{sc} increased to 6.41 mA cm^{-2} under illumination, with a fill factor (FF) of 0.66 and an efficiency of 2.66%. The N3 dye absorbs visible light, as shown in its UV-Vis spectrum, and the light-excited electrons from N3
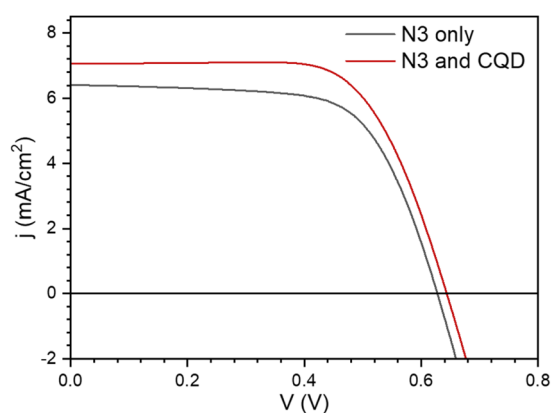
inject into the conduction band of TiO$_2$, ultimately reaching the FTO layer. This mechanism explains the j–V curve observed under light conditions. When both N3 dye and CQDs were used, the J_{sc} increased to 7.05 mA cm^{-2}, and the FF and η improved to 0.68 and 3.08%, respectively. This suggests that while CQDs alone act as a weak sensitizer, their combination with N3 induces a substantial increase in J_{sc}, highlighting a synergistic effect. CQDs function as a one-way electron transfer mediator, forming a bridge between N3 and the TiO$_2$ substrate. Similar mechanisms have been reported in previous studies.[42] Compared with previous studies,[40,41] which reported efficiency improvements of 12.3% (from 7.30% to 8.20%) and 5.0% (from 7.80% to 8.19%) using the N-719 dye, the results from this study validate the effectiveness of CQDs synthesized by the hydrothermal method in enhancing DSSC performance.

Mechanism of CQDs synthesis

The reaction mechanism between nutshells and H$_2$O$_2$ for CQD production is illustrated in Fig. 12. In this reaction, H$_2$O$_2$ serves as an oxidant, a role it has been widely employed for in various applications, such as pollutant degradation, due to its low environmental impact. Although H$_2$O$_2$ is not a particularly strong oxidizing agent, its reaction with pure organic matter is generally slow and requires high activation energy.[43] However, the presence of inorganic metal ions can act as catalysts in this process when nutshells react with H$_2$O$_2$ under hydrothermal conditions. Specifically, metal ions such as Fe^{2+}, which are initially bound within the organic material, are released into the solution during the reaction. This release facilitates the formation of Fenton's reagent *in situ*. Iron is a well-known Fenton catalyst and exhibits high reactivity with H$_2$O$_2$.[44] In the presence of Fe^{2+}, H$_2$O$_2$ decomposes to produce hydroxyl radicals (·OH), which possess a standard redox potential of 2.8 V—significantly higher than that of H$_2$O$_2$ itself. These hydroxyl
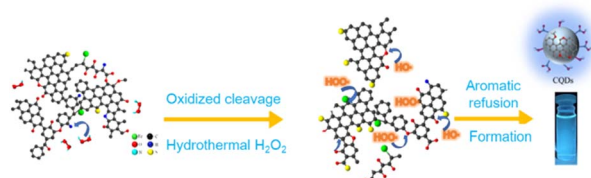

Fig. 11 j–V curves of solar cells where the electro anodes were treated by: TiO$_2$ paste only (blank), TiO$_2$ paste plus either one of CQD or N3 dye or both.

Fig. 12 A proposed schematic reaction to produce CQDs from nutshells *via* the H$_2$O$_2$ hydrothermal method.

radicals (·OH) exhibit strong oxidative capabilities and selectively abstract electrons from the organic material. Initially, unsaturated organic groups in the nutshell undergo oxidation. Additionally, hydrogen substitution reactions between the free radicals (·OH) and saturated organic compounds also take place. Free radicals (·OH) can further interact with the benzene rings and R–H groups, resulting in the formation of R$^{·}$ radicals through hydrogen abstraction. These R$^{·}$ radicals can then participate in additional reactions, promoting further degradation of the organic material. In the Fenton reaction mechanism, the R$^{·}$ radicals react with oxygen-containing compounds, generating $HO_2^{·}/O_2^{·-}$ species that can further facilitate the conversion of Fe^{2+} and accelerate the decomposition of the nutshell. As a result, the large organic structures, including macromolecular polycyclic aromatic compounds, are broken down and converted into nanosized carbon particles, ultimately forming CQDs in the solution. Additionally, smaller carbon molecules with aromatic structures recombine and grow into CQDs under the hydrothermal conditions.

Conclusions

This study presents an environmentally friendly and efficient method for synthesizing carbon quantum dots (CQDs) from nutshells, a renewable and widely available biomass waste. By utilizing a hydrothermal reaction with H_2O_2 as the oxidizing agent, we successfully synthesized CQDs exhibiting exceptional photoluminescent properties and excellent dispersion in aqueous solutions. Optimization of key synthesis parameters—specifically temperature, reaction time, and H_2O_2 concentration—was crucial in achieving CQDs with a narrow size distribution and an average diameter of approximately 3 nm. The byproducts of the reaction, including gas, liquid, and solid residues, were systematically collected and analyzed to provide a comprehensive understanding of the synthesis process. When incorporated into dye-sensitized solar cells (DSSCs), the synthesized CQDs demonstrated significant improvements in photovoltaic performance, particularly in terms of enhanced short-circuit current density and overall energy conversion efficiency. This underscores the potential of CQDs as efficient light-harvesting materials. Moreover, the presence of inorganic catalysts, such as Fe^{2+}, during the synthesis was identified as a key factor in accelerating the reaction rate and minimizing oxygen-related by-products. These findings emphasize the critical role of biomass composition in CQD synthesis and highlight the potential of utilizing waste materials in sustainable nanomaterial production.

Data availability

Data available within the article. And the raw data of this article can be obtained by contacting the corresponding author.

Author contributions

Yang Yu: methodology, writing – original draft, Yuxia Ouyang: validation, software, data curation, Fei Xu: software, data curation, Tiefeng Wang: data curation, Xiaoyan Wei: project administration, resources, Tongtong Wang: writing – review editing, conceptualization, methodology, funding acquisition, Yi Yao: writing – review editing, conceptualization, methodology.

Conflicts of interest

There are no conflicts to declare.

Acknowledgements

References

1 S. Zhang, S.-F. Jiang, B.-C. Huang, X.-C. Shen, W.-J. Chen, T.-P. Zhou, H.-Y. Cheng, B.-H. Cheng, C.-Z. Wu and W.-W. Li, *Nat. Sustainability*, 2020, **3**, 753–760.

2 S. Ganguly, P. Das, S. Banerjee and N. C. Das, *Funct. Compos. Struct.*, 2019, **1**, 022001.

3 H.-L. Yang, L.-F. Bai, Z.-R. Geng, H. Chen, L.-T. Xu, Y.-C. Xie, D.-J. Wang, H.-W. Gu and X.-M. Wang, *Mater. Today Adv.*, 2023, **18**, 100376.

4 M. N. Mustafa and Y. Sulaiman, *Sol. Energy*, 2020, **212**, 332–338.

5 P. Das, S. Ganguly, S. Banerjee and N. C. Das, *Res. Chem. Intermed.*, 2019, **45**, 3823–3853.

6 T. F. Yadeta and T. Imae, *Appl. Surf. Sci.*, 2023, **637**, 157880.

7 M. N. Mustafa and Y. Sulaiman, *J. Electroanal. Chem.*, 2020, **876**, 114516.

8 S. K. Saraswat, M. A. Mustafa, G. K. Ghadir, M. Kaur, D. F. G. Lozada, A. M. Al-Ani, M. Y. Alshahrani, M. K. Abid, S. S. Jumaa and D. Y. Alhameedi, *Inorg. Chem. Commun.*, 2024, 112279.

9 S. Tajik, Z. Dourandish, K. Zhang, H. Beitollahi, Q. Van Le, H. W. Jang and M. Shokouhimehr, *RSC Adv.*, 2020, **10**, 15406–15429.

10 P. Russo, R. Liang, E. Jabari, E. Marzbanrad, E. Toyserkani and Y. N. Zhou, *Nanoscale*, 2016, **8**, 8863–8877.

11 B. Han, M. Yu, T. Pen, Y. Li, X. Hu, R. Xiang, X. Hou and G. He, *New J. Chem.*, 2017, **41**, 5267–5270.

12 X. Li and Z. Zhao, *RSC Adv.*, 2014, **4**, 57615–57619.

13 S. Mallakpour and V. Behranvand, *J. Cleaner Prod.*, 2018, **190**, 525–537.

14 Z.-y. Yan, A. Xiao, H. Lu, Z. Liu and J.-q. Chen, *New Carbon Mater.*, 2014, **29**, 216–224.

15 S. P. Sasikala, L. Henry, G. Yesilbag Tonga, K. Huang, R. Das, B. Giroire, S. Marre, V. M. Rotello, A. Penicaud, P. Poulin and C. Aymonier, *ACS Nano*, 2016, **10**, 5293–5303.

16 L. Li, C. Liu, Y. Qiu, N. Mitsuzak and Z. Chen, *Int. J. Hydrogen Energy*, 2017, **42**, 19654–19663.

17 A. Chae, Y. Choi, S. Jo, N. a. Nur'aeni, P. Paoprasert, S. Y. Park and I. In, *RSC Adv.*, 2017, **7**, 12663–12669.

18 P. Namdari, B. Negahdari and A. Eatemadi, *Biomed. Pharmacother.*, 2017, **87**, 209–222.

19 J. Prekodravac, B. Vasiljević, Z. Marković, D. Jovanović, D. Kleut, Z. Špitalský, M. Mičušik, M. Danko, D. Bajuk-Bogdanović and B. Todorović-Marković, *Ceram. Int.*, 2019, **45**, 17006–17013.

20 A. Das, N. Bar and S. K. Das, *J. Colloid Interface Sci.*, 2020, **580**, 245–255.

21 L. Liu, X. Yu, Z. Yi, F. Chi, H. Wang, Y. Yuan, D. Li, K. Xu and X. Zhang, *Nanoscale*, 2019, **11**, 15083–15090.

22 C. Manterola-Barroso, D. Padilla Contreras, G. Ondrasek, J. Horvatinec, G. Gavilán CuiCui and C. Meriño-Gergichevich, *Plants*, 2024, **13**, 1034.

23 L. Wang, S. Weng, S. Su and W. Wang, *RSC Adv.*, 2023, **13**, 19173–19194.

24 X. Wang, L. Xu, S. Ge, S. Y. Foong, R. K. Liew, W. W. F. Chong, M. Verma, M. Naushad, Y.-K. Park and S. S. Lam, *Energy*, 2023, **274**, 127354.

25 M. Jouyandeh, S. S. M. Khadem, S. Habibzadeh, A. Esmaeili, O. Abida, V. Vatanpour, N. Rabiee, M. Bagherzadeh, S. Iravani and M. R. Saeb, *Green Chem.*, 2021, **23**, 4931–4954.

26 J. Escalante, W.-H. Chen, M. Tabatabaei, A. T. Hoang, E. E. Kwon, K.-Y. A. Lin and A. Saravanakumar, *Renewable Sustainable Energy Rev.*, 2022, **169**, 112914.

27 W.-H. Chen and P.-C. Kuo, *Energy*, 2011, **36**, 6451–6460.

28 D. Díez, A. Urueña, R. Piñero, A. Barrio and T. Tamminen, *Processes*, 2020, **8**, 1048.

29 F. Liu, Y. Zhang, S. Wang, T. Gong, M. Hua, J. Qian and B. Pan, *Chem. Eng. J.*, 2022, **430**, 132767.

30 L. Zhang, B. Zhan, S. Zhang, H. Ji, S. Peng, M. Fan and L. Yan, *Green Chem.*, 2025, **27**, 1789.

31 T. Wang, A. H. Rony, K. Sun, W. Gong, X. He, W. Lu, M. Tang, R. Ye, J. Yu, L. Kang, H. Luo, S. J. Smith, E. G. Eddings and M. Fan, *Cell Rep. Phys. Sci.*, 2020, **1**, 100079.

32 M. Rani, U. Shanker, B. S. Kaith and M. Sillanpää, *Inorg. Chem. Commun.*, 2024, **159**, 111878.

33 D. Ozyurt, M. A. Kobaisi, R. K. Hocking and B. Fox, *Carbon Trends*, 2023, **12**, 100276.

34 G. Kalaiyarasan, C. Hemlata and J. Joseph, *ACS Omega*, 2019, **4**, 1007–1014.

35 W. You, W. Zou, S. Jiang, J. Zhang, Y. Ge, G. Lu, D. W. Bahnemann and J. H. Pan, *Carbon Neutralization*, 2024, **3**, 245–284.

36 L. Wang, W. Li, L. Yin, Y. Liu, H. Guo, J. Lai, Y. Han, G. Li, M. Li and J. Zhang, *Sci. Adv.*, 2020, **6**, eabb6772.

37 N. Liu, J. Liu, W. Kong, H. Li, H. Huang, Y. Liu and Z. Kang, *J. Mater. Chem. B*, 2014, **2**, 5768–5774.

38 P. K. Praseetha, R. I. J. Litany, H. M. Alharbi, A. A. Khojah, S. Akash, M. Bourhia, A. A. Mengistie and G. A. Shazly, *Sci. Rep.*, 2024, **14**, 24435.

39 S. Dua, P. Kumar, B. Pani, A. Kaur, M. Khanna and G. Bhatt, *RSC Adv.*, 2023, **13**, 13845–13861.

40 R. Riaz, M. Ali, T. Maiyalagan, A. S. Anjum, S. Lee, M. J. Ko and S. H. Jeong, *Appl. Surf. Sci.*, 2019, **483**, 425–431.

41 Y. Zhang, Y. Zhao, J. Duan and Q. Tang, *Electrochim. Acta*, 2018, **261**, 588–595.

42 M. N. Mustafa and Y. Sulaiman, *Sol. Energy*, 2021, **215**, 26–43.

43 Q. Wang, H. Guo, H. Wang, M. A. Urynowicz, A. Hu, C.-P. Yu, P. Fallgren, S. Jin, H. Zheng and R. J. Zeng, *Fuel*, 2019, **236**, 1345–1355.

44 E. C. Lumbaque, D. S. Araújo, T. M. Klein, E. R. L. Tiburtius, J. Argüello and C. Sirtori, *Catal. Today*, 2019, **328**, 259–266.